Thieme

Investigation of the Metabolism of Astragaloside IV in a Puromycin-Damaged Rat Model by UPLC-Q-TOF-MS/MS Analysis

Authors
Bing Zhang[1*], Shiying Huang[2*], Zhuoting Liu[3], Xinhui Liu[1], Zilan Jiang[3], Jianping Chen[2], Youjia Zeng[1]

Affiliations
1 Department of Nephrology, Shenzhen Traditional Chinese Medicine Hospital, The Fourth Clinical Medical College of Guangzhou University of Chinese Medicine, Shenzhen, Guangdong, China
2 Shenzhen Key Laboratory of Hospital Chinese Medicine Preparation, Shenzhen Traditional Chinese Medicine Hospital, The Fourth Clinical Medical College of Guangzhou University of Chinese Medicine, Shenzhen, Guangdong, China
3 The Fourth Clinical Medical College, Guangzhou University of Chinese Medicine, Shenzhen, China

Key words
Astragalus membranaceus, Fabaceae, astragaloside IV, metabolite profiling, UPLC-Q-TOF-MS/MS, puromycin aminonucleoside

received	October 26, 2022
accepted after revision	September 28, 2023
published online	November 6, 2023

Bibliography
Planta Med 2024; 90: 154–165
DOI 10.1055/a-2186-3182
ISSN 0032-0943

Georg Thieme Verlag KG, Rüdigerstraße 14, 70469 Stuttgart, Germany

Correspondence
Prof. Youjia Zeng
Shenzhen Traditional Chinese Medicine Hospital
Via Fuhua Road 1#, Futian Area, 518033 Shenzhen, Guangdong Province, China
Phone: + 86 (0) 7 55 82 73 23 04, Fax: + 86 (0) 7 55 88 35 60 33
rainlucy@126.com

Correspondence
Prof. Jianping Chen
Shenzhen Traditional Chinese Medicine Hospital
Via Fuhua Road 1#, Futian Area, 518033 Shenzhen, Guangdong Province, China
Phone: + 86 (0) 7 55 82 73 23 04, Fax: + 86 (0) 7 55 88 35 60 33
lycjp@126.com

Supplementary material is available under https://doi.org/10.1055/a-2186-3182

ABSTRACT

Astragaloside IV (AS-IV) has been shown to provide renal protection in various kidney injury models. However, the metabolic profile variation of AS-IV in pathological models *in vivo* is not well established. This study aims to explore the metabolic pathway of AS-IV *in vivo* in the classical puromycin aminonucleoside (PAN)-induced kidney injury in a rat model. Twelve Wistar rats were randomly divided into the AS-IV (CA) and the PAN+AS-IV (PA) treatment groups. PAN was injected by a single tail intravenous (i. v.) injection at 5 mg/100 g body weight, and AS-IV was administered intragastrically (i. g.) at 40 mg/kg for 10 days. Fecal samples of these rats were collected, and metabolites of AS-IV were detected by ultra-performance liquid chromatography coupled with quadrupole/time-of-flight mass spectrometry (UPLC-Q-TOF-MS/MS) to explore the AS-IV metabolic pathway. The metabolic differences between the AS-IV and PAN+AS-IV groups were compared. A total of 25 metabolites were detected, and deglycosylation, deoxygenation, and methyl oxidation were found to be the main metabolic pathways of AS-IV *in vivo*. The abundance of most of these metabolites in the PAN+AS-IV group was lower than that in the AS-IV treatment group, and differences for seven of them were statistically significant. Our study indicates that AS-IV metabolism is affected in the PAN-induced kidney injury rat model.

Introduction

Chronic kidney disease (CKD) is a progressive disease with high morbidity and mortality characterized by the irreversible damage of kidney structure and function owing to various causes. A recent study reported that the prevalence of CKD reached up to 13.4% globally, driven by an ageing population and an increasing incidence of diabetes and obesity [1, 2]. Moreover 11% of CKD patients with stage 3 will eventually develop end-stage renal disease

* Co-first authors.

ABBREVIATIONS

AS-IV	astragaloside IV
PAN	puromycin aminonucleoside
i. v.	intravenous
i. g.	intragastrically
UPLC-Q-TOF-MS/MS	ultra-performance liquid chromatography coupled with quadrupole/time-of-flight mass spectrometry
CA	control+AS-IV
PA	PAN+AS-IV
CKD	chronic kidney disease
ESRD	end-stage renal disease
WHO	World Health Organization
XIC	extracted ion chromatogram
TIC	total ion chromatogram
m/z	mass-to-charge ratio
TMAO	trimethylamine N-oxide
LAB	lactic acid bacteria

(ESRD) [3]. The annual and global number of deaths from CKD reported to the World Health Organization (WHO) was estimated at 5–10 million [4]. Furthermore, with the progress of the disease, the economic burden of CKD increases. A retrospective cohort study from 2008 to 2020 reported that overall mean healthcare costs, regardless of CKD stage, were £5401 per patient per year in England [5]. CKD has become a leading public health problem globally. Therefore, the need for an effective intervention to prevent progressive CKD is urgent.

Astragaloside IV (AS-IV) is a bioactive component in Astragali Radix, the root of *Astragalus membranaceus* (Fisch.) Bge. var. *mongholicus* (Bge.) Hsiao or *Astragalus membranaceus* (Fisch.) Bge. (Fabaceae). AS-IV (3-*O*-*β*-D-xylopyranosyl-6-*O*-*β*-D-glucopyranosyl-cycloastragenol) is a cycloartane-type triterpene glycoside. Several studies have reported the beneficial effects of AS-IV on multiple kidney disease models such as diabetic nephropathy [6], unilateral ureteral occlusion-induced renal fibrosis [7], ischemia/reperfusion (IR)-induced renal injury [8], lipopolysaccharide-induced acute kidney injury [9], and chronic glomerulonephritis [10]. According to our previous findings, oral administration of AS-IV (40 mg/kg) to rats for 10 days alleviated the kidney injury caused by a single intravenous injection (in the tail vein) of puromycin aminonucleoside (PAN) (5 mg/100 g body weight) via activating the Wnt/PCP pathway [11]. However, AS-IV metabolism and biotransformation *in vivo* have not been elucidated in PAN-induced kidney models.

Ultra-performance liquid chromatography coupled with quadrupole/time-of-flight mass spectrometry (UPLC-Q-TOF-MS/MS) is a powerful method for metabolite analysis because of its accuracy and sensitivity and has been widely used in exploring the drug behavior *in vivo* from absorption to excretion [12]. This advanced technique helped to profile AS-IV metabolites in rat plasma, bile, urine, and feces, from which 22 major metabolites were detected [13]. The major metabolic reactions were hydrolysis, glucuronidation, sulfation, and dehydrogenation. Kong et al. [14] used UPLC-Q-TOF-MS/MS and surface-enhanced Raman spectroscopy to characterize four different Astragalus saponins and their metabolites after oral administration in rats. However, AS-IV metabolism and biotransformation in disease models has been rarely studied yet.

In this study, we used UPLC-Q-TOF-MS/MS to detect AS-IV metabolites in the PAN-induced kidney injury rat model for the exploration of metabolic pathways, which should help to further understand AS-IV metabolism in disease states. The effect of PAN on AS-IV's metabolic process was examined by comparing the metabolic profiles of the AS-IV and PAN+AS-IV groups.

Results

In this study, ultra-performance liquid chromatography–quadrupole time-of-flight-mass spectrometry (UPLC-Q-TOF-MS/MS) was employed to investigate the metabolites of AS-IV in a fecal sample. Twenty-five metabolites were identified and annotated using the MetabolitePilot 2.0.4 software. The authenticity of AS-IV was verified by comparing it with a reference standard. Information on the identified metabolites, such as their retention times, proposed elemental compositions, and characteristic fragment ions, is shown in ▶ **Table 1**. The extracted ion chromatogram (XIC) and the representative total ion chromatogram (TIC) of fecal sample 1 from the AS-IV group (CA), PAN+AS-IV group (PA), and the background control are presented in ▶ **Figs. 1** and **2**. The structures of the metabolites were determined by comparing their mass spectral fragmentation data with literature data or AS-IV. Each metabolite was analyzed as described in the Supporting Information, which includes the mass spectra and fragment description.

The peak that eluted at 7.78 min had a similar protonated molecular ion, MS-fragmentation, and chromatographic behavior to those of the AS-IV standard. Full-scan MS analyses of AS-IV showed an intense $[M + H]^+$ peak at *m/z* 785.4682 and four isotopic peaks (*m/z* 785.9692, 786.4712, 787.4738, and 788.4774). A fragment was observed at *m/z* 143.1056, indicating a loss of $C_8H_{15}O_2$ from the parent ion, followed by the elimination of H_2O to produce the ion at *m/z* 125.0954. The characteristic fragmentation pattern of AS-IV includes the successive loss of glucose, xylose, and H_2O molecules, producing ions with *m/z* 605.4024, 587.3421, and 455.3499, respectively. Additionally, the compound can directly lose glucose and xylose, resulting in the generation of the ion at *m/z* 473.3606. The ions with *m/z* 437.3390 and 419.3292 were produced by loss of two H_2O molecules from *m/z* 473.3606 and 455.3499, respectively (▶ **Fig. 3 a, b**). These fragmentation patterns were essential for the identification of the metabolites of AS-IV.

Based on the observation of the quasi-molecular $[M + H]^+$ ion at *m/z* 653.4222, the molecular formula of the metabolite M4 was inferred to be $C_{36}H_{60}O_{10}$. The mass of M4 was 132 Da lower than the parent drug, suggesting it to be a partially deglycosylated metabolite of AS-IV [13]. Referring to PubChem database, M4 might be brachyoside B (PubChem CID: 14 241 109)

Metabolites M17 and M18 had an identical mass ion $[M + H]^+$ at *m/z* 491.3713 and 491.3712, respectively, and eluted at 10.43 and 11.12 min, respectively. Typical MS^2 ions with *m/z* 143.1062 and 125.0960 were observed during their fragmentation.

▶ **Table 1** Metabolites of astragaloside IV in rat feces detected by UPLC-Q-TOF-MS analysis.

Peak ID	Identity	Formula	*m/z*	R. T. (min)	Δppm	Fragment ions (*m/z*)	Metabolic reaction from AS-IV
M1	Loss of $C_6H_{10}O_5$ and $C_5H_8O_4$+ methyl oxidation to carboxylic acid	$C_{30}H_{48}O_7$	521.3464	6.37	− 1.8	107.0853, 123.1153, 125.0948, 127.1121, 143.1057, 297.2202, 485.3243, 503.3346	deglycosylation, methyl oxidation
M2	Loss of $C_6H_{10}O_5$ and $C_5H_8O_4$+ methyl oxidation to carboxylic acid	$C_{30}H_{48}O_7$	521.3464	6.59	− 1.8	123.0792, 125.0951, 143.1052, 401.2724, 419.2920, 431.2913, 437.3012, 449.3031, 467.3136, 485.3239, 503.3338	deglycosylation, methyl oxidation
M3	Loss of $C_6H_{10}O_6$ and $C_5H_8O_5$+ methyl oxidation to carboxylic acid	$C_{30}H_{48}O_5$	489.3556	6.64	− 3.8	107.0829, 123.1164, 125.0949, 127.1098, 143.1053, 297.2190, 95.0832, 411.3229, 417.3109, 435.3217, 453.3327, 471.3112	deglycosylation, methyl oxidation
M4	Loss of $C_5H_8O_4$	$C_{36}H_{60}O_{10}$	653.4222	7.48	− 5.7	165.1262, 177.0525, 211.1321, 353.2400, 371.2563, 389.2672, 407.2813	deglycosylation
M5	Loss of O	$C_{41}H_{68}O_{13}$	769.4724	7.84	− 1.1	133.0493, 295.0947, 409.3344, 421.3433, 439.3511, 441.3708, 457.3670, 571.3883, 589.4093, 607.4134, 751.3755, 751.4062, 751.4794	deoxygenation
M6	Loss of $C_6H_{10}O_6$ and $C_5H_8O_4$+ methyl oxidation to carboxylic acid	$C_{30}H_{48}O_6$	505.3513	8.16	− 2.2	147.1168, 189.1271, 253.1941, 271.2053, 311.2370, 337.2521, 393.2767, 411.2869, 433.3081, 451.3186, 469.3295, 487.3390	deglycosylation, methyl oxidation
M7	Loss of O	$C_{41}H_{68}O_{13}$	769.4723	8.20	− 1.2	279.2223, 297.2398, 329.2442, 439.3590, 751.4901	deoxygenation
M8	Methylation	$C_{42}H_{70}O_{14}$	799.4826	8.42	− 1.6	143.1062, 355.2601, 437.3346	methylation
M9	Loss of $C_6H_{10}O_5$ and $C_5H_8O_4$+ methyl oxidation to carboxylic acid	$C_{30}H_{48}O_7$	521.3458	9.20	− 2.8	71.0479, 125.0951, 127.1112, 135.1136, 143.1059, 449.3048, 467.3149, 485.3281, 503.3253	deglycosylation, methyl oxidation
M10	Oxidation	$C_{41}H_{66}O_{14}$	783.4459	9.22	− 8.5	373.2698, 393.1661	oxidation
M11	Loss of $C_6H_{10}O_6$ and $C_5H_8O_5$+ methyl oxidation to carboxylic acid	$C_{30}H_{48}O_5$	489.3546	9.25	− 5.9	107.0853, 123.1162, 125.0963, 127.1115, 141.1275, 143.1058, 173.1323, 417.3127, 435.3243, 453.3323, 471.3426	deglycosylation, methyl oxidation

continued

▶ **Table 1** *Continued*

Peak ID	Identity	Formula	*m/z*	R.T. (min)	Δppm	Fragment ions (*m/z*)	Metabolic reaction from AS-IV
M12	Loss of $C_6H_{10}O_6$ and $C_5H_8O_4$+ methyl oxidation to carboxylic acid	$C_{30}H_{48}O_6$	505.3508	9.38	−3.1	107.0846, 123.1147, 125.0952, 127.1125, 143.1058, 297.2179, 315.2307, 393.2771, 421.3090, 433.3072, 439.3203, 451.3179, 469.3291, 487.3387	deglycosylation, methyl oxidation
M13	Loss of $C_6H_{10}O_5$ and $C_5H_8O_4$+ Oxidation	$C_{30}H_{50}O_6$	507.3652	9.55	−5.5	125.0950, 143.1060, 157.1007, 173.1311, 377.2811, 405.3146, 417.3105, 423.3119, 435.3227, 453.3284, 471.3393, 489.3432	deglycosylation and oxidation
M14	Loss of $C_6H_{10}O_6$ and $C_5H_8O_5$	$C_{30}H_{50}O_3$	459.3815	9.77	−3.8	81.0696, 149.0968, 173.1326, 175.1487, 187.1479, 189.1640, 201.1637, 215.1785, 219.1752, 367.2969, 389.3200, 407.3265, 425.3367, 443.3468	
M15	Loss of $C_6H_{10}O_6$ and $C_5H_8O_4$	$C_{30}H_{50}O_4$	475.3763	10.06	−3.9	205.1585, 421.3107, 439.3221, 457.3293	deglycosylation
M16	Loss of $C_6H_{10}O_6$ and $C_5H_8O_5$+ methyl oxidation to carboxylic acid	$C_{30}H_{48}O_5$	489.3557	10.38	−3.7	125.0950, 143.1070, 145.1014, 173.1318, 185.1323, 253.1945, 271.2050, 417.3124, 435.3232, 453.3336, 471.3431	deglycosylation, methyl oxidation
M17	Loss of $C_6H_{10}O_5$ and $C_5H_8O_4$	$C_{30}H_{50}O_5$	491.3713	10.43	−3.7	71.0493, 125.0960, 143.1062, 419.3288, 437.3385, 455.3502, 473.3587	deglycosylation
M18	Loss of $C_6H_{10}O_5$ and $C_5H_8O_4$	$C_{30}H_{50}O_5$	491.3712	11.12	−4.0	71.0490, 125.0953, 419.3299, 437.3383, 455.3502, 473.3541	deglycosylation
M19	Loss of $C_6H_{10}O_6$ and $C_5H_8O_4$	$C_{30}H_{50}O_4$	475.3760	11.33	−4.5	95.0852, 193.1584, 219.1743, 263.1994, 273.2216, 399.3225, 421.3437, 439.3540, 457.3650	deglycosylation
M20	Loss of $C_6H_{10}O_6$ and $C_5H_8O_5$+ methyl oxidation to carboxylic acid	$C_{30}H_{48}O_5$	489.3559	11.65	−3.1	125.0953, 173.1311, 187.1469, 199.1473, 201.1631, 417.3131, 435.3231, 453.3335, 471.3438	deglycosylation, methyl oxidation
M21	Loss of O	$C_{41}H_{68}O_{13}$	769.4713	12.47	−2.5	120.0833, 350.2308, 479.3448, 507.3407, 725.4456, 733.4268, 751.4653, 751.4936, 751.5253, 751.5704	deoxygenation
M22	Loss of $C_6H_{10}O_6$ and $C_5H_8O_4$	$C_{30}H_{50}O_4$	475.3760	12.93	−4.6	81.0695, 109.1001, 123.1159, 193.1585, 273.2173, 291.2314, 421.3428, 439.3551, 457.3644	deglycosylation

continued

▶ **Table 1** *Continued*

Peak ID	Identity	Formula	*m/z*	R. T. (min)	Δppm	Fragment ions (*m/z*)	Metabolic reaction from AS-IV
M23	Loss of $C_5H_8O_5$+ methyl oxidation to carboxylic acid	$C_{36}H_{58}O_{11}$	667.4001	13.86	− 7.6	147.0630, 341.0159, 429.0906, 479.8299	methyl oxidation
M24	Loss of $C_6H_{10}O_6$	$C_{35}H_{58}O_8$	607.4183	14.08	− 3.6	165.0899, 431.3857, 455.3732, 465.3550, 571.4313	deglycosylation
M25	Loss of $C_6H_{10}O_6$ and $C_5H_8O_4$	$C_{30}H_{50}O_4$	475.3780	15.05	− 0.4	109.1006, 119.0838, 121.0998, 123.1162, 133.0998, 173.1312, 291.2343, 439.3568, 457.3571	deglycosylation

All data were collected in positive ion mode.

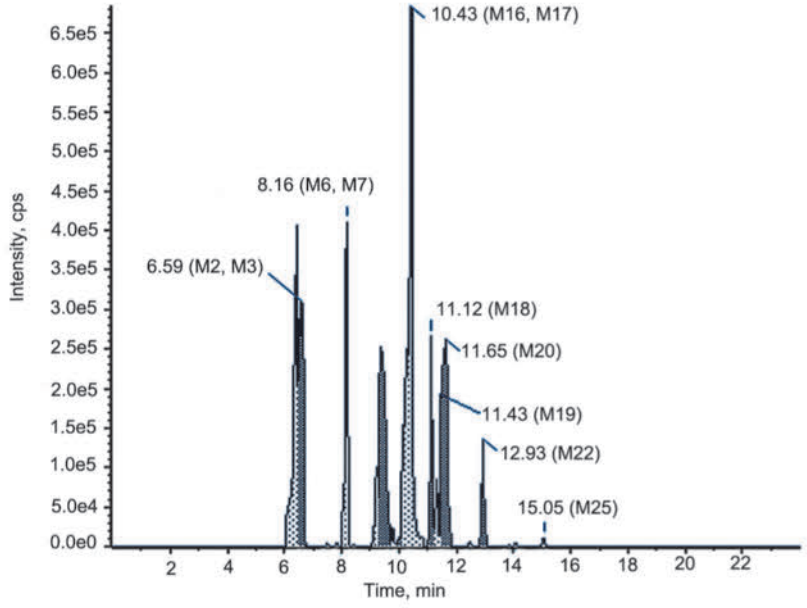

▶ **Fig. 1** Representative XIC chromatograms of rat samples after intragastric administration of 40 mg/kg astragaloside IV.

Their molecular formula was determined to be $C_{30}H_{50}O_5$ owing to the loss of $C_6H_{10}O_5$ (162 Da) from M4, indicating that M17 and M18 were deglycosylation metabolites of AS-IV. Referring to Jin et al. [15], Zhou et al. [16], and the PubChem database, M17 and M18 might be cycloastragenol (PubChem CID: 13 943 286) and 3-epi-cycloastragenol, which have been reported to be metabolites of AS-IV produced by the intestinal microbiota.

Metabolites M1, M2, and M9 had retention times of 6.37 min, 6.59 min, and 9.20 min, respectively. The metabolites showed a protonated molecular $[M + H]^+$ ion at *m/z* 521.3464, 521.3464, and 521.3458, respectively, corresponding to the molecular formula of $C_{30}H_{48}O_7$. These three metabolites originated from M17 and M18, following methyl oxidation to a carboxylic acid. The fragment ions at *m/z* 485.3243 and 503.3346 were generated by the successive loss of H_2O from *m/z* 521.3464. Furthermore, ions with *m/z* 143.1057 and 125.0948 were observed during the fragmentation process. Hence, M1, M2, and M9 were identified as isomeric deglycosylation and methyl oxidation products of AS-IV. However, the detailed mechanisms for the formation of these isomers are yet unknown.

Four metabolites, namely M3, M11, M16, and M20, were detected with $[M + H]^+$ protonated molecular ions at *m/z* 489.3556, 489.3546, 489.3557, and 489.3559, respectively. They eluted at 6.64, 9.25, 10.38, and 11.65 min and had a molecular formula of $C_{30}H_{48}O_5$ corresponding to a loss of 2 Da from M17 or M18. Furthermore, the diagnostic ions at *m/z* 143.1058 and 125.0963 were observed during the fragmentation process, along with a neutral loss of 18 Da (H_2O). Thus, two metabolites might be oxi-

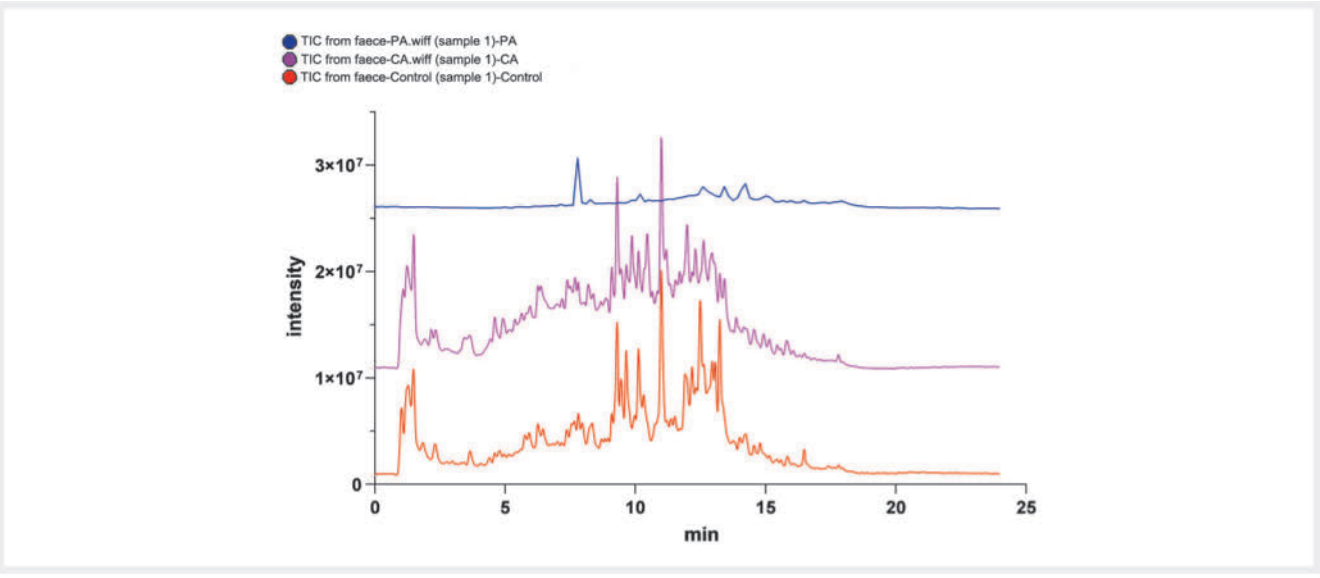

▶ **Fig. 2** Representative TIC of fecal sample 1 from AS-IV group (CA), PAN+AS-IV group (PA), and background control.

dation products of cycloastragenol and its isomer, while the remaining two remained unidentified [16].

Metabolites M5, M7, and M21 had retention times of 7.84 min, 8.20 min, and 12.47 min, respectively. The molecular formula of these three metabolites was determined to be $C_{41}H_{68}O_{13}$ based on their precursor $[M + H]^+$ ion at *m/z* 769.4724, 769.4723, and 769.4713, respectively. Their mass was 16 Da lower than that of the parent drug, suggesting them to be deoxygenated metabolites of AS-IV. Furthermore, characteristic mass fragments with *m/z* 589.4093 and 441.3708 were also observed, which was attributed to the loss of glucose and xylose.

Metabolites M6 and M12 had retention times of 8.16 min and 9.38 min, respectively. The $[M + H]^+$ ions of M6 and M12 were observed at *m/z* 505.3513 and 505.3508, respectively, indicating a molecular formula of $C_{30}H_{48}O_6$ corresponding to the elimination of 280 Da from the parent drug. They were formed by the loss of $C_5H_8O_4$ (132 Da) and $C_6H_{10}O_6$ (178 Da) from AS-IV and methyl oxidation to carboxylic acid. A typical MS^2 fragmentation with ions at *m/z* 487.3390 and 469.3295 was attributed to the successive loss of H_2O. Hence, M6 and M12 resulted from deglycosylation of AS-IV and methyl oxidation to carboxylic acid.

Metabolite M8 had a retention time of 8.42 min. Its molecular formula was determined to be $C_{42}H_{70}O_{14}$ based on the observed protonated molecular ion $[M + H]^+$ at 799.4826. Its mass was 14 Da higher than the parent drug, revealing methylation. Moreover, a characteristic ion was observed at *m/z* 143.1062.

Metabolite M10 was detected at 9.22 min and had a molecular formula of $C_{41}H_{66}O_{14}$, revealed by an $[M + H]^+$ protonated ion at 783.4459. This metabolite had a 2 Da lower mass than the parent drug, indicating it to be an oxidation metabolite of AS-IV.

Metabolite M13 ($C_{30}H_{50}O_6$) was observed at a retention time of 9.55 min with a protonated molecular ion $[M + H]^+$ at 507.3652. This metabolite was an oxidation product of M17 and M18. Additionally, we observed MS^2 ions at *m/z* 489.3432, 471.3393, 453.3284, and 435.3227, which could be attributed to the successive loss of four H_2O molecules. Therefore, M13 was produced by the loss of $C_6H_{10}O_5$ (162 Da) and $C_5H_8O_4$ (132 Da) from AS-IV and subsequent oxidation.

Metabolite M14 had a retention time of 9.77 min. The $[M + H]^+$ protonated molecular ion was observed at 459.3815 Da, corresponding to the molecular formula of $C_{30}H_{50}O_3$. We identified two cleavage pathways leading to the formation of M14. The first pathway involved the loss of $C_5H_8O_5$ (148 Da) from M24, while the second pathway involved the loss of O (16 Da) from M15, M19, M22, and M25.

Metabolites M15, M19, M22, and M25 had the same molecular formula, $C_{30}H_{50}O_4$, and were detected at retention times of 10.06, 11.33, 12.93, and 15.05 min, respectively. Their $[M + H]^+$ precursor ions were observed at *m/z* 475.3763, 475.3760, 475.3760, and 475.3780, respectively, which was 310 Da lower than the parent drug, thereby indicating that AS-IV had lost $C_6H_{10}O_6$ (178 Da) and $C_5H_8O_4$ (132 Da) to yield these four metabolites. MS^2 ions with *m/z* 457.3293, 439.3221, and 421.3107 were observed, which could be attributed to the successive loss of three H_2O molecules. Hence, M15, M19, M22, and M25 were deglycosylation metabolites of AS-IV. Moreover, two of these four metabolites could also be produced from M17/18, a pair of isomers, owing to losing 16 Da (O). However, the other two metabolites remained unidentified.

Metabolite M23 eluted at 13.86 min and had a molecular formula of $C_{36}H_{58}O_{11}$ based on its $[M + H]^+$ protonated molecular ion observed at 667.4001 Da, which was 118 Da lower than the parent drug. This indicated that AS-IV had lost $C_5H_8O_5$ (148 Da) and undergone methyl oxidation to carboxylic acid to yield M23.

Metabolite M24 was detected at a retention time of 14.08 min and had a molecular formula of $C_{35}H_{58}O_8$. Its $[M + H]^+$ protonated molecular ion was observed at *m/z* 607.4183, indicating a loss of 178 Da corresponding to $C_6H_{10}O_6$ from AS-IV.

The total ion chromatogram (TIC) revealed that M17 and M6 were the main metabolites. Metabolite M17 had a retention time

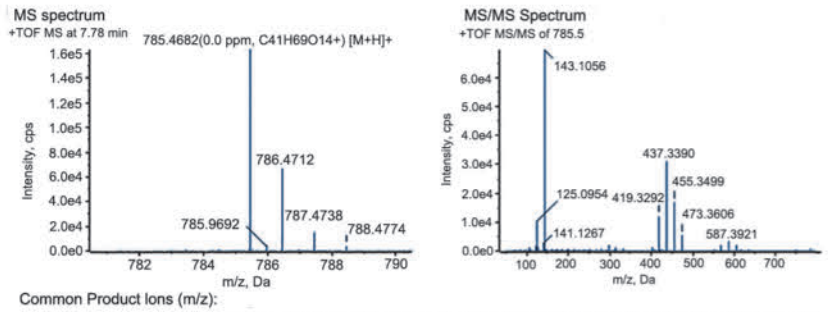

Common Product Ions (m/z):

107.0849, 123.1162, 125.0954, 127.1108, 141.1267, 143.1056, 297.2208, 315.2314, 419.3292, 437.3390, 455.3499, 473.3606, 569.3819, 587.3921, 605.4024

a

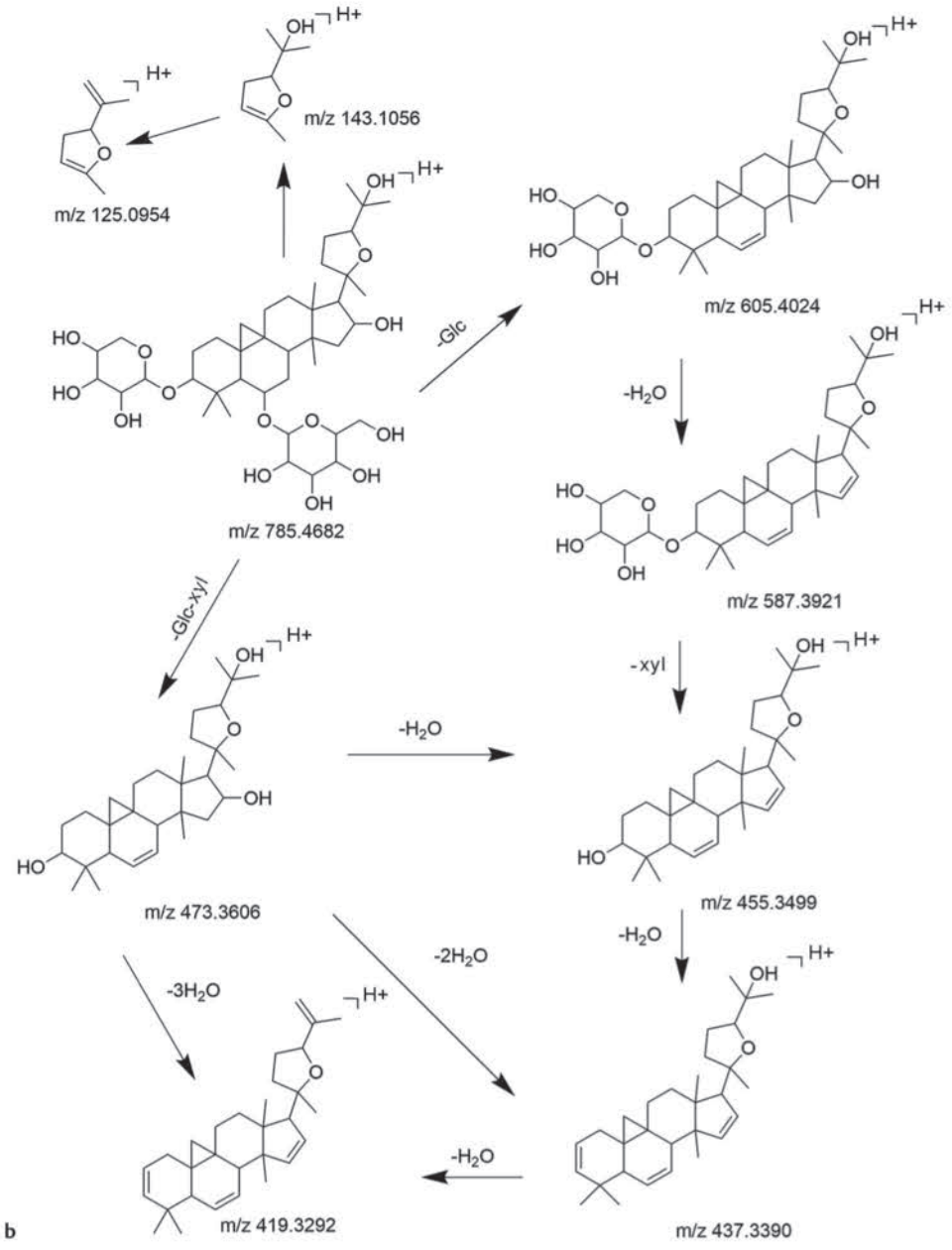

b

▶ **Fig. 3** **a** MS and MS/MS spectra of astragaloside IV. **b** Fragmentation pattern of astragaloside IV.

of 10.43 min and was identified by the precursor ion $[M + H]^+$ observed at *m/z* 491.3713. This metabolite had a molecular formula of $C_{30}H_{50}O_5$ and was formed by the loss of 162 Da ($C_6H_{10}O_5$) and 132 Da ($C_5H_8O_4$) from the parent drug. Hence, M17 was a deglycosylation metabolite of AS-IV. M6 ($C_{30}H_{48}O_6$) was the methyl oxidation product following the deoxygenation of the M17. Therefore, deglycosylation, deoxygenation, and methyl oxidation were the main metabolic pathways of AS-IV in rats (▶ **Fig. 4**).

We compared the metabolic profiles of AS-IV between the AS-IV (CA) and PAN+AS-IV (PA) groups. We found that the PA group showed lower levels of most of the fecal metabolites than the CA group (▶ **Fig. 5**), and the difference in the levels of M1, M6, M7, M9, M12, M18, and M19 corresponding to deglycosylation, deoxygenation and methyl oxidation metabolites of AS-IV showed statistical significance (▶ **Table 2**).

Discussion

The underlying biochemical mechanisms of CKD are not fully clear and could involve lipid metabolism [17], purine metabolism, amino acid biosynthesis, tryptophan metabolism, or neuroactive ligand–receptor interaction disorder [18]. These metabolism disturbances have partly been shown to be mediated through metabolites of gut microbiota. Mo et al. [19] found that abundance of Coprococcus_3 was positively correlated with serum level of trimethylamine N-oxide (TMAO), which is a kind of uremic toxin that is produced by gut microbiota from dietary precursors, including phosphatidylcholine, choline, and betaine [20, 21]. Elevated plasma levels of TMAO and its precursors are associated with poor prognosis of CKD [22]. Da-Yong Hu et al. reported that inhibiting the TMAO biosynthetic pathway attenuated renal injury in a murine model of CKD [23]. Yan-Ni Wang et al. demonstrated that the dysregulation of phosphatidylcholine metabolism is involved in CKD pathology [17]. Betaine was also related to kidney function and identified as the potential plasma metabolic biomarker for predicting urate nephropathy [24]. Thus, the gut microbiota may be the origin of the abnormal serum metabolites associated with CKD and its complications [19].

Astragalus was first recorded in "Shen Nong's Materia Medica". AS-IV is an important bioactive component of Astragalus and has many effects, such as anti-oxidation, anti-inflammatory, anti-apoptosis, and anti-fibrosis properties, as well as intestinal regulatory and immunomodulatory effects [25]. Several studies have reported the pharmacological effects of AS- IV *in vitro* and *in vivo*. Zhao et al. [26] showed AS-IV-mediated inhibition of ROS-related endoplasmic reticulum stress and TXNIP/NLRP3 inflammasome activation. He et al. [27] reported that AS-IV enhanced the intestinal transit time in slow-transit constipation mice by modulating their gut microbiota and generating butyrate. However, limited studies have reported on the metabolism of AS-IV. Early studies showed a cumulative recovery rate of 52.14% of AS-IV in urine and feces [28], indicating that ~ 50% of it is metabolized in the body, which supports our findings, but further study of its metabolites and metabolic mechanism has yet to be conducted. A study by Sun et al. [29] has shown that AS-IV is mainly metabolized by the intestinal flora and undergoes glycosyl hydrolysis *in vitro*. A study on rats' metabolism of cycloastragenol found seven, six, and one phase I metabolites in their feces, urine, and bile, respectively, but no phase II metabolites were detected [30]. Cheng et al. [13] profiled the AS-IV metabolites in rat plasma, bile, urine, and feces by UPLC-Q-TOF-MS/MS. The major metabolic reactions of AS-IV involved hydrolysis, glucuronidation, sulfation, and dehydrogenation and showed biotransformation *in vivo*. AS-IV generated 22 metabolites during the phase I and phase II metabolic reactions. Our study detected 25 metabolites and showed deglycosylation, deoxygenation, and methyl oxidation to carboxylic acid as the main metabolic pathways of AS-IV in rats. The metabolic reactions of AS-IV are believed to be primarily influenced by the intestinal flora. According to Takeuchi et al. [31], lactic acid bacteria (LAB) and bifidobacteria in the gut could metabolize AS-IV to cycloastragenol. As for the final products, bifidobacteria produced CA, while LAB produced 20R,24S-epoxy-6α,16β,25-trihydroxy-9,19-cycloartan-3-one (cycloastragenol-2H). In the puromycin-damaged rat model, we found lower fecal metabolites in the PA group compared to the CA group. These findings suggest that the rat gut microbiota or metabolic enzyme profiles change in nephrotic syndrome. Further studies are needed to explore the relevant mechanisms.

In summary, 25 metabolites of AS-IV were detected in rat feces by UPLC-Q-TOF-MS/MS. The main metabolic pathways of AS-IV *in vivo* are deglycosylation, deoxygenation, and methyl oxidation to carboxylic acid. PAN-induced nephrotic syndrome status may affect the metabolism of AS-IV.

Materials and Methods

Chemicals and Reagents

AS-IV (purity > 98% as determined by HPLC) was purchased from ChengDu Conbon Biotech Co., Ltd. PAN (purity > 99%) was purchased from MedChemExpress. Sodium carboxyl methyl cellulose (CMC-Na) was supplied by Sinopharm Chemical Reagents. Formic acid, acetonitrile, and methanol (Merck) were of HPLC grade. Water was from a Milli-Q Ultrapure Water system (Millipore).

Animals

Male Wistar rats (n = 12) weighing 150–180 g were purchased from the Experimental Animal Center of Southern Medical University. They were randomly divided into two groups: the AS-IV group (n = 6) and PAN + AS-IV group (n = 6). Before experimentation, the rats were acclimatized for 2 days in metabolic cages and fed standard chow and water. Blank feces samples were collected for 24 h. On day 3, 5 mg/100 g body weight of PAN was injected into the tail intravenously (i. v.), and AS-IV was administered intragastrically (i. g.) at 40 mg/kg for 10 days. Fecal samples were collected for 24 h and stored at − 70 °C until further analysis. The animal study was reviewed and approved by the Experimental Animal Ethics Committee of Guangzhou University of Chinese Medicine on April 10th, 2020 (Approval No. 20 200 401 052).

Fecal Sample Processing

Methanol (5 mL) was added to the fecal (0.5 g) samples and vortexed for 5 min, followed by ultrasonication for 30 min using a KQ5200 Ultrasonic Cleaner (Kunshan Ultrasonic Instruments).

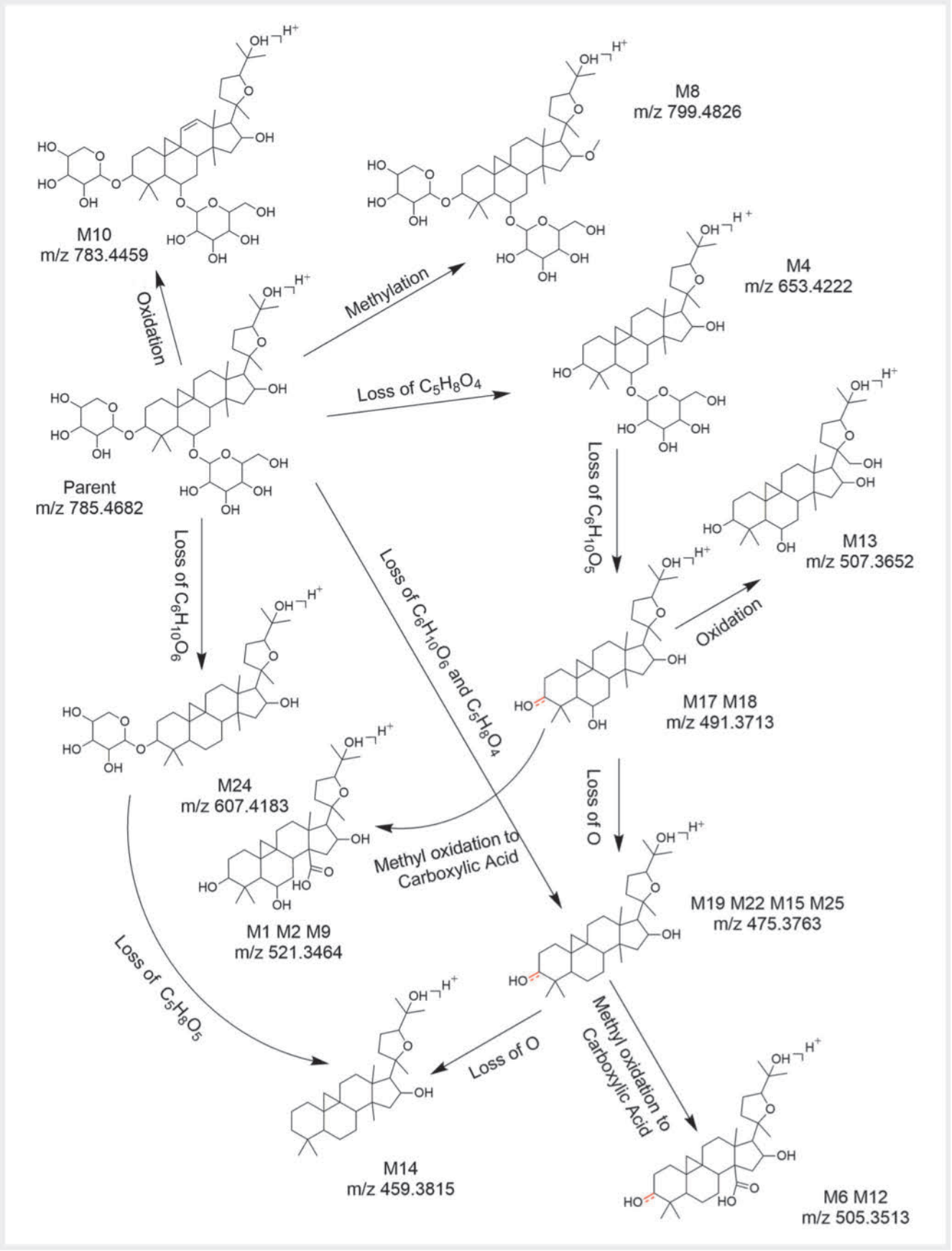

▶ **Fig. 4** Proposed major metabolic pathway of astragaloside IV. Stereoisomers at C-3 are indicated with a bond in red.

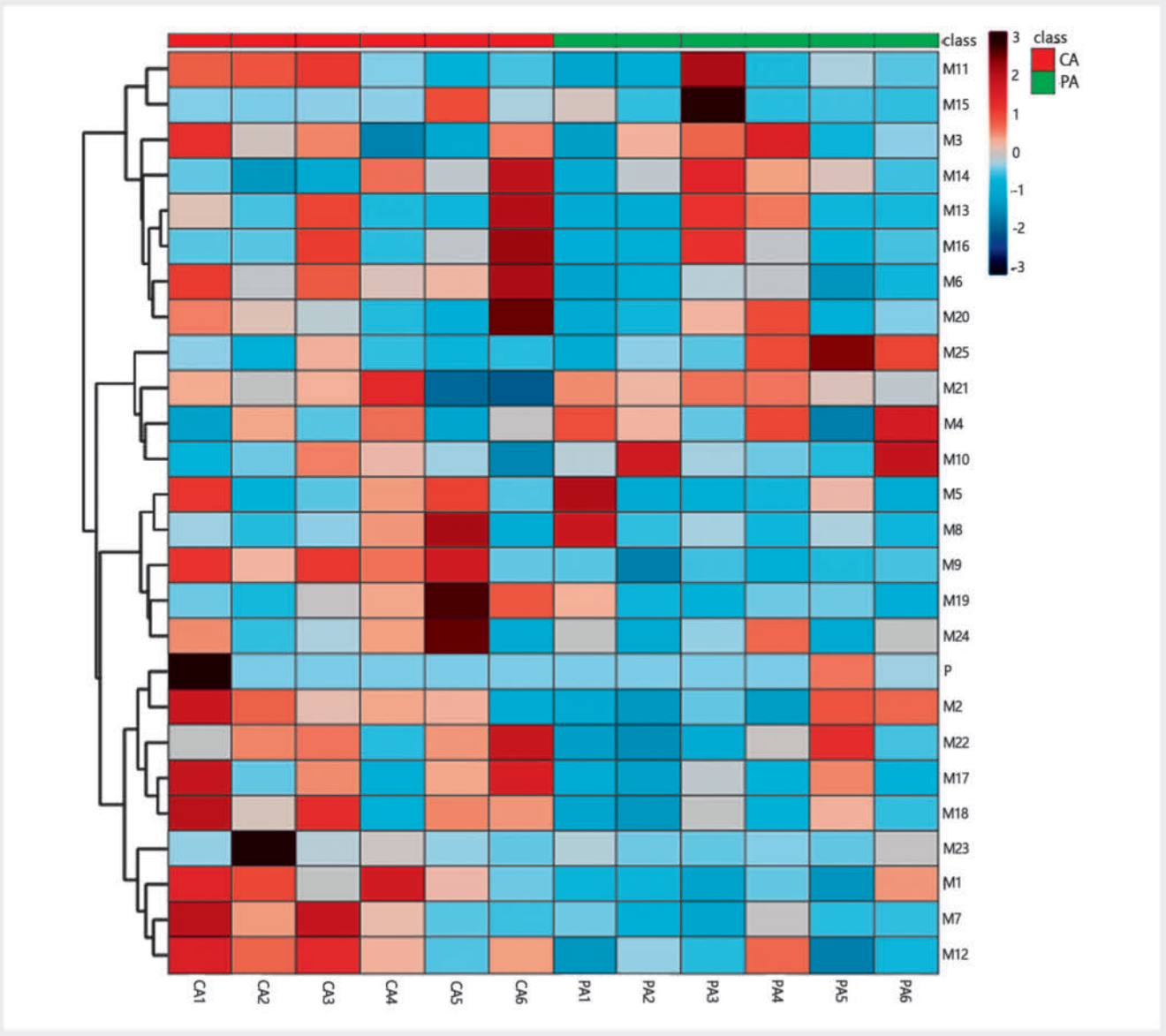

▶ **Fig. 5** Comparison of astragaloside IV metabolites between PA and CA groups. CA, AS-IV group; PA, PAN + AS-IV group; P, AS-IV.

Then, the mixture was centrifuged at 3000 × g for 10 min at 4 °C. The supernatants were collected and dried under nitrogen gas at 37 °C. Afterward, 1 mL of methanol was added to redissolve the sample, and the samples were filtered through 0.22 µm membranes (Millipore). Then, 2 µL of the filtered sample was injected into the UPLC-Q-TOF-MS/MS system.

UHPLC-Q-TOF-MS/MS Analysis

Chromatographic separation was performed on a SCIEX Exion LC system (AB Sciex). UHPLC conditions were as follows: Waters Acquity BEH C18 column (2.1 × 100 mm, 1.7 µm); column temperature: 30 °C; mobile phase: 0.1% formic acid in water (A) and acetonitrile (B); gradient conditions: 0–4 min 10–13% B; 4–6 min 13–50% B; 6–10 min 50% B; 10–14 min 50–85% B; 14–18 min 85% B; 18–20 min 85–100%; 20–25 min 100%; flowrate: 0.2 mL/min; injection volume: 2 µL. MS detection was performed on a X500B Q-TOF mass spectrometer (AB Sciex), which was operated in positive ion mode (ESI^+). The MS parameters were as follows: gas1 and gas2, 45 psi; curtain gas, 35 psi; heat block temperature, 550 °C; ion spray voltage, 5.5 kV; declustering potential, 50 V; collision energy, ± 35 V; and the collision energy spread (CES) was ± 15 V.

Data Processing

Data were processed with SCIEX OS version 2.2.0 (AB SCIEX). The results of the drug-contained samples were compared using MetabolitePilot 2.0.4 software (AB SCIEX) with a list of potential metabolites. Metabolites were detected and identified automatically.

▶ **Table 2** Mann–Whitney U assay for content of astragaloside IV metabolites.

Label	p Value	Fold change
M1	0.02*	0.62
M2	0.24	0.74
M3	0.94	1.03
M4	0.31	1.25
M5	0.24	0.73
M6	0.00**	0.49
M7	0.03*	0.48
M8	0.94	0.85
M9	0.00**	0.49
M10	0.31	1.58
M11	0.39	0.85
M12	0.03*	0.55
M13	0.24	0.70
M14	0.82	1.02
M15	0.31	1.33
M16	0.24	0.59
M17	0.13	0.42
M18	0.04*	0.44
M19	0.04*	0.40
M20	0.48	0.65
M21	0.48	1.22
M22	0.13	0.56
M23	0.24	0.18
M24	0.59	0.57
M25	0.24	2.61
P	0.82	0.33

* $p < 0.05$; ** $p < 0.01$, fold change is PA/CA

Statistical Analysis

Statistical analysis was performed using SPSS statistics software version 16.0 (SPSS Inc.). Comparison of the two groups was carried out using the Mann–Whitney U test. $P < 0.05$ indicates statistical significance.

Supporting Information

The mass spectra of metabolites and fragment description of M1–M25 are available in Supporting Information.

Contributors' Statement

Data collection: B. Zhang, S. Y. Huang, X. H. Liu, Z. T. Liu; design of the study: Y. J. Zeng, J. P. Chen, B. Zhang, S. Y. Huang; statistical analysis: J. P. Chen, X. H. Liu, Z. T. Liu, S. Y. Huang; analysis and interpretation of the data: B. Zhang, Y. J. Zeng, S. Y. Huang; drafting the manuscript: B. Zhang, S. Y. Huang; critical revision of the manuscript: Y. J. Zeng, J. P. Chen.

Acknowledgements

The authors are thankful to the Natural Science Foundation of Guangdong Province (2017A030313518) and the Sanming Project of Medicine in Shenzhen (No. SZZYSM202111002).

Conflict of Interest

The authors declare that they have no conflict of interest.

References

[1] Hill NR, Fatoba ST, Oke JL, Hirst JA, O'Callaghan CA, Lasserson DS, Hobbs FD. Global prevalence of chronic kidney disease – A systematic review and meta-analysis. PLoS One 2016; 11: e0158765

[2] Kovesdy CP. Epidemiology of chronic kidney disease: An update 2022. Kidney Int Suppl 2022; 12: 7–11

[3] Humphreys BD. Mechanisms of renal fibrosis. Annu Rev Physiol 2018; 80: 309–326

[4] Luyckx VA, Tonelli M, Stanifer JW. The global burden of kidney disease and the sustainable development goals. Bull World Health Organ 2018; 96: 414D–422D

[5] Pollock C, James G, Garcia Sanchez JJ, Carrero JJ, Arnold M, Lam CSP, Chen HT, Nolan S, Pecoits-Filho R, Wheeler DC. Healthcare resource utilisation and related costs of patients with CKD from the UK: A report from the DISCOVER CKD retrospective cohort. Clin Kidney J 2022; 15: 2124–2134

[6] Feng H, Zhu X, Tang Y, Fu S, Kong B, Liu X. Astragaloside IV ameliorates diabetic nephropathy in db/db mice by inhibiting NLRP3 inflammasome-mediated inflammation. Int J Mol Med 2021; 48: 164

[7] Cao Y, Zhang L, Wang Y, Fan Q, Cong Y. Astragaloside IV attenuates renal fibrosis through repressing epithelial-to-mesenchymal transition by inhibiting microRNA-192 expression: *In vivo* and *in vitro* studies. Am J Transl Res 2019; 11: 5029–5038

[8] Xin Y, Li G, Liu H, Ai D. AS-IV protects against kidney IRI through inhibition of NF-κB activity and PUMA upregulation. Int J Clin Exp Med 2015; 8: 18293–18301

[9] Zhou W, Chen Y, Zhang X. Astragaloside IV alleviates lipopolysaccharide-induced acute kidney injury through down-regulating cytokines, CCR5 and p-ERK, and elevating anti-oxidative ability. Med Sci Monit 2017; 23: 1413–1420

[10] Lu R, Chen J, Liu B, Lin H, Bai L, Zhang P, Chen D, Li H, Li J, Pang Y, Zhou Y, Zhou J, Wu J. Protective role of astragaloside IV in chronic glomerulonephritis by activating autophagy through PI3K/AKT/AS160 pathway. Phytother Res 2020; 34: 3236–3248

[11] Zeng Y, Zhang B, Liu X, He L, Wang T, Yu X, Kang Y, Li S. Astragaloside IV alleviates puromycin aminonucleoside-induced podocyte cytoskeleton injury through the Wnt/PCP pathway. Am J Transl Res 2020; 12: 3512–3521

[12] Shi Z, Jiang J, Zhao D, Xie B, Li Y, Yu C. Effects of astragaloside IV on the pharmacokinetics of metoprolol in rats and its mechanism. Curr Drug Metab 2022; 23: 131–136

[13] Cheng XD, Wei MG. Profiling the metabolism of astragaloside IV by ultra performance liquid chromatography coupled with quadrupole/time-of-flight mass spectrometry. Molecules 2014; 19: 18881–18896

[14] Kong S, Ou S, Liu Y, Xie M, Mei T, Zhang Y, Zhang J, Wang Q, Yang B. Surface-enhanced raman spectroscopy analysis of astragalus saponins and identification of metabolites after oral administration in rats by ul-

trahigh-performance liquid chromatography/quadrupole time-of-flight mass spectrometry analysis. Front Pharmacol 2022; 13: 828449

[15] Jin Y, Guo X, Yuan B, Yu W, Suo H, Li Z, Xu H. Disposition of astragaloside IV via enterohepatic circulation is affected by the activity of the intestinal microbiome. J Agric Food Chem 2015; 63: 6084–6093

[16] Zhou RN, Song YL, Ruan JQ, Wang YT, Yan R. Pharmacokinetic evidence on the contribution of intestinal bacterial conversion to beneficial effects of astragaloside IV, a marker compound of astragali radix, in traditional oral use of the herb. Drug Metab Pharmacokinet 2012; 27: 586–597

[17] Wang YN, Zhang ZH, Liu HJ, Guo ZY, Zou L, Zhang YM, Zhao YY. Integrative phosphatidylcholine metabolism through phospholipase A(2) in rats with chronic kidney disease. Acta Pharmacol Sin 2023; 44: 393–405

[18] Li H, Zhang H, Yan F, He Y, Ji A, Liu Z, Li M, Ji X, Li C. Kidney and plasma metabolomics provide insights into the molecular mechanisms of urate nephropathy in a mouse model of hyperuricemia. Biochim Biophys Acta Mol Basis Dis 2022; 1868: 166374

[19] Mo Y, Sun H, Zhang L, Geng W, Wang L, Zou C, Wu Y, Ji C, Liu X, Lu Z. Microbiome-metabolomics analysis reveals the protection mechanism of α-Ketoacid on adenine-induced chronic kidney disease in rats. Front Pharmacol 2021; 12: 657827

[20] Wang Z, Klipfell E, Bennett BJ, Koeth R, Levison BS, Dugar B, Feldstein AE, Britt EB, Fu X, Chung YM, Wu Y, Schauer P, Smith JD, Allayee H, Tang WH, DiDonato JA, Lusis AJ, Hazen SL. Gut flora metabolism of phosphatidylcholine promotes cardiovascular disease. Nature 2011; 472: 57–63

[21] Tang WH, Wang Z, Levison BS, Koeth RA, Britt EB, Fu X, Wu Y, Hazen SL. Intestinal microbial metabolism of phosphatidylcholine and cardiovascular risk. N Engl J Med 2013; 368: 1575–1584

[22] Gupta N, Buffa JA, Roberts AB, Sangwan N, Skye SM, Li L, Ho KJ, Varga J, DiDonato JA, Tang WHW, Hazen SL. Targeted inhibition of gut microbial trimethylamine N-oxide production reduces renal tubulointerstitial fibrosis and functional impairment in a murine model of chronic kidney disease. Arterioscler Thromb Vasc Biol 2020; 40: 1239–1255

[23] Hu DY, Wu MY, Chen GQ, Deng BQ, Yu HB, Huang J, Luo Y, Li MY, Zhao DK, Liu JY. Metabolomics analysis of human plasma reveals decreased production of trimethylamine N-oxide retards the progression of chronic kidney disease. Br J Pharmacol 2022; 179: 4344–4359

[24] Janssen EM, Dy SM, Meara AS, Kneuertz PJ, Presley CJ, Bridges JFP. Analysis of patient preferences in lung cancer – estimating acceptable tradeoffs between treatment benefit and side effects. Patient Prefer Adherence 2020; 14: 927–937

[25] Zhang J, Wu C, Gao L, Du G, Qin X. Astragaloside IV derived from astragalus membranaceus: A research review on the pharmacological effects. Adv Pharmacol 2020; 87: 89–112

[26] Zhao Y, Li Q, Zhao W, Li J, Sun Y, Liu K, Liu B, Zhang N. Astragaloside IV and cycloastragenol are equally effective in inhibition of endoplasmic reticulum stress-associated TXNIP/NLRP3 inflammasome activation in the endothelium. J Ethnopharmacol 2015; 169: 210–218

[27] He Q, Han C, Huang L, Yang H, Hu J, Chen H, Dou R, Ren D, Lin H. Astragaloside IV alleviates mouse slow transit constipation by modulating gut microbiota profile and promoting butyric acid generation. J Cell Mol Med 2020; 24: 9349–9361

[28] Du Y, Zhang Q, Chen GG, Wei P, Tu CY. Pharmacokinetics of astragaloside IV in rats by liquid chromatography coupled with tandem mass spectrometry. Eur J Drug Metab Pharmacokinet 2005; 30: 269–273

[29] Sun GX, Zhao YY, Miao PP, Yang XY, Miao Q, Li J, Xue BJ, Su J, Zhang YJ. Stability study in biological samples and metabolites analysis of astragaloside IV in rat intestinal bacteria in vitro. Zhongguo Zhong Yao Za Zhi 2014; 39: 4258–4264

[30] Ma PK, Wei BH, Cao YL, Miao Q, Chen N, Guo CE, Chen HY, Zhang YJ. Pharmacokinetics, metabolism, and excretion of cycloastragenol, a potent telomerase activator in rats. Xenobiotica 2017; 47: 526–537

[31] Takeuchi DM, Kishino S, Ozeki Y, Fukami H, Ogawa J. Analysis of astragaloside IV metabolism to cycloastragenol in human gut microorganism, bifidobacteria, and lactic acid bacteria. Biosci Biotechnol Biochem 2022; 86: 1467–1475